

Interstitial Flow Promotes Macrophage Polarization toward an M2 Phenotype

Ran Li¹, Jean Carlos Serrano², Hao Xing¹, Tara A. Lee¹, Hesham Azizgolshani², Muhammad Zaman³, and Roger D. Kamm^{1,2,*}

Corresponding Author:

Roger D. Kamm

Departments of Mechanical Engineering and Biological Engineering

77 Massachusetts Avenue, Rm. NE47-321

Cambridge, MA 02139

Email: rdkamm@mit.edu

Telephone: 617-253-5330

Abstract

Tumor tissues are characterized by an elevated interstitial fluid flow from the tumor to the surrounding stroma. Macrophages in the tumor microenvironment are key contributors to tumor progression. While it is well established that chemical stimuli within the tumor tissues can alter macrophage behaviors, the effects of mechanical stimuli, especially the flow of interstitial fluid in the tumor microenvironment, on macrophage phenotypes have not been explored. Here, we used 3D biomimetic models to reveal that macrophages can sense and respond to pathophysiological levels of interstitial fluid flow reported in tumors ($\sim 3 \mu\text{m/s}$). Specifically, interstitial flow (IF) polarizes macrophages toward an M2-like phenotype via integrin/Src-mediated mechanotransduction pathways involving STAT3/6. Consistent with this flow-induced M2 polarization, macrophages treated with IF migrate faster and have an enhanced ability to promote cancer cell migration. Moreover, IF directs macrophages to migrate against the flow. Since IF emanates from the tumor to the surrounding stromal tissues, our results suggest that IF could not only induce M2 polarization of macrophages, but also recruit these M2 macrophages toward the tumor masses, contributing to cancer cell invasion and tumor progression. Collectively, our study reveals that IF could be a critical regulator of tumor immune environment.

Highlight Summary

Solid tumor tissues are characterized by an elevated interstitial fluid flow from the tumor to the surrounding stroma. In this study, we found that this flow can polarize macrophages toward a tumor-supportive M2 phenotype and direct macrophages to migrate against the flow via mechanotransduction pathways.

Introduction

Cancer is a complex disease that depends not only on cancer cells themselves but also on the environment in which they reside. This environment, collectively termed the tumor microenvironment (TME), consists of non-cancerous stromal cells and biophysical forces (Quail and Joyce, 2013; Wirtz et al., 2011). Extensive evidence suggests that TME can contribute to malignancy. Specifically, macrophages, one of the most abundant tumor-associated stromal cell types, play critical roles in tumor invasion and metastasis (Condeelis and Pollard, 2006). Macrophages are innate immune cells that can rapidly adopt a broad spectrum of phenotypes based on the stimuli they encounter in their surroundings. At one extreme, these functionally plastic cells can polarize toward a pro-inflammatory M1 phenotype, while at the other extreme, an immunosuppressive M2 phenotype (Mantovani et al., 2002). Macrophages in the TME often skew toward M2 states, and the number of M2-like macrophages that have infiltrated near or into the tumor tissues has been found to correlate with poor prognosis (Leek et al., 1996). Indeed, M2-like macrophages in tumors can produce various growth factors and cytokines that promote metastasis by enhancing tumor cell invasion, intravasation, and immune escapes (Lewis and Pollard, 2006; Mantovani et al., 2002). In contrast, M1-like macrophages in tumors are thought to induce tumor suppression by activating anti-tumor immunity (Noy and Pollard, 2014). Since the roles that macrophages (M1 vs. M2) play in tumor progression make them attractive targets for anti-tumor therapy (Noy and Pollard, 2014), it is important to understand how the TME regulates macrophage phenotypes.

A myriad of chemical stimuli in the tumor microenvironment can control macrophage behaviors. For example, IFN γ produced by NK cells is known to skew macrophages toward an M1 phenotype (O'Sullivan et al., 2012), allowing these macrophages to secrete pro-inflammatory cytokines (TNF α , IL1, and IL12) that promote a sustained, anti-tumor response from NK cells, Th1 cells, and cytotoxic T cells

(Panni et al., 2013). In contrast, IL4 and CSF-1 secreted by Th2 cells and tumor cells can co-opt macrophages to adopt an M2-like phenotype and produce molecules, such as TGF β and IL10, that drive tumor progression (Noy and Pollard, 2014). Although the roles that chemical factors play in macrophage polarization are well studied (Mantovani et al., 2002), whether mechanical stimuli, an equally important but often underappreciated component of tumor microenvironment, affect macrophage phenotypes remains an open question.

One of the most prominent tumor-associated mechanical factors is interstitial flow (IF), and clinical data have demonstrated that elevated IF in the tumor tissues correlates with poor patient outcomes (Nathanson and Nelson, 1994). Indeed, IF has been shown to promote tumor progression by influencing the migration of cancer cells and fibroblasts. This flow of interstitial fluid through the extracellular matrix (ECM) is the result of fluid pressure gradients and lymphatic drainage within the tissue (Heldin et al., 2004). In the malignant tissue, the build-up of fluid in the tumor core increases fluid pressure gradients near the tumor margin, resulting in high levels of IF emanating from the tumor and draining into the surrounding stroma (Swartz and Lund, 2012). This elevated IF, a hallmark of cancer, ranges from 1-5 $\mu\text{m/s}$, and is highest at the tumor/stromal boundary (Heldin et al., 2004; Hompland et al., 2012). As tumor-associated macrophages tend to reside near this boundary (Lewis and Pollard, 2006; Ohno et al., 2004; Wyckoff et al., 2007), it is believed that they can experience an elevated IF *in vivo*, underscoring the need to consider IF in studying the tumor immune environment. Nevertheless, the effects of this crucial tumor-associated biophysical force on macrophages, a key immune cell type in the TME, have not been explored.

In the present study, we used 3D microfluidic tissue culture systems to mimic tumor-associated interstitial flow ($\sim 3 \mu\text{m/s}$) and study the effects of interstitial flow on macrophages cultured in a 3D collagen I ECM. We demonstrate, for the first time, that IF enhances the M2 polarization of macrophages by up-regulating the expression of M2 markers Arg I, TGF β , CD206, CD163, and TGM2, all of which have been shown to be expressed by macrophages in tumors (Afik et al., 2016; Krneta et al., 2017;

Quatromoni and Eruslanov, 2012; Sharda et al., 2011; Zhang et al., 2017). In addition, we show that IF promotes macrophage migration, as well as the ability of macrophages to induce cancer cell invasion, characteristics that are consistent with that of the tumor-associated M2 macrophages. Our mechanistic analysis reveals that this flow-induced M2-like phenotype is dependent on $\beta 1$ integrin/Src-mediated STAT3/6 activation. Interestingly, we also found that interstitial flow directs the migration of macrophages against the direction of flow (upstream). Since IF emanates from the tumor to the surrounding stromal tissues, these results suggest that IF could enhance tumor progression by promoting not only macrophage polarization toward the M2 phenotype, but also the recruitment of these M2-like macrophages from the stromal tissues toward the tumor mass.

Results

Interstitial flow (IF) polarizes macrophages toward an M2 phenotype in 3D ECM

To study the effects of interstitial flow (IF) on macrophages, we first used a 3D microfluidic model consists of a PDMS microfluidic system with two large media reservoirs attached to the top of the microfluidic chamber (Figures 1A and S1A) (Haessler et al., 2012; Polacheck et al., 2014). We cultured macrophages within a 3D collagen I ECM embedded in the central gel region, flanked by two media channels that were connected to reservoirs via media ports (Figure 1A). A media-height difference of 1.5 mm was established between the two reservoirs to generate a hydrostatic pressure gradient across the gel region (Figure S1A), which we estimated, based on the measured collagen gel hydraulic permeability of $7 \times 10^{-14} \text{ m}^2$ and Darcy's law, to drive interstitial fluid flow with a mean velocity of $\sim 3 \text{ } \mu\text{m/s}$ through the collagen gel containing macrophages (*Material and Methods, Interstitial Flow Calculation*). We chose the velocity of $3 \text{ } \mu\text{m/s}$ to mimic the level of IF in the tumor tissues measured *in vivo* (Hompland et al., 2012). Since the microfluidic device is optically transparent, macrophage behaviors (i.e. morphology, protein expression, and migration) in response to the IF treatment can be readily assessed (Figure 1B), and IF velocity can be quantified by tracking the trajectory of micro-beads flowing through the collagen

gel region in the device (Figure 1C). Using fluorescent micro-beads, we verified that the velocity of IF experienced by macrophages in our microfluidic system, consistent with the numerical prediction computed from Darcy's law, was indeed $\sim 3 \mu\text{m/s}$ (Figure S1B). Moreover, since the cross-sectional area of the media reservoirs is 2000 times that of the collagen gel, no appreciable changes in media-height difference (data not shown) or IF velocity (Figure S1B) were observed during the course of 24 hours.

M2 macrophages inside the tumor tissues can promote metastasis and tumor progression by enhancing tumor angiogenesis and migration (Mantovani et al., 2002). Since elevated IF has been shown to correlate with metastasis (Swartz and Lund, 2012), we hypothesized that IF could promote macrophage M2 polarization. To test this hypothesis, we treated bone marrow-derived macrophages (BMDMs), using the microfluidic device, with IF for 48 hrs in the absence of any externally applied chemical stimulus, and we assessed the effects of IF on the expression of macrophage polarization markers. We first verified that IF treatment did not alter the viability of macrophages as assessed through live/dead assay (Figure S2). Subsequent immunofluorescent staining revealed that IF treatment significantly up-regulated the expressions of M2 markers (CD163, CD206) in macrophages seeded in the device (Figure 1D). To further verify this result, we conducted experiments in a 3D transwell flow chamber to determine if IF can induce macrophage expression of M2 markers using western blot analysis. Macrophages were seeded inside a 2.5 mg/mL collagen I gel in the transwell insert and a media-height difference of 10 mm was maintained across the gel by a recirculating pump, producing an IF of $\sim 3 \mu\text{m/s}$ through the collagen gel containing macrophages (Figure 1E). We found that 48-hr IF treatment of macrophages in the flow chamber resulted in an enhanced expression of macrophage M2 markers TGF β , Arginase I (ArgI), TGM2, and CD206 by 2-13 fold (Figures 1F-G). Moreover, IF induced the expression of these M2 markers to levels that are similar to that of IL4 treatment (Figure S3). In contrast, IF did not significantly affect the expression of the M1 markers (CD86, iNOS, and TNF α) compared to the no-flow control (Figures 1D, F-G). Since IF treatment resulted in the up-regulation of multiple M2 markers in two different experimental models

(microfluidic system and transwell flow chamber), we conclude that IF can polarize macrophages toward an M2 phenotype.

IF induces M2 polarization via β 1 integrin/Src-mediated activation of STAT3/6

To further probe the molecular mechanisms of flow-induced M2 polarization, we tested the effects of IF on the activation of the transcription factors that regulate macrophage phenotypes, namely STAT3, STAT6, and STAT1. STAT3 and 6 are transcription factors that control the production of M2-associated proteins in macrophages (Niemand et al., 2003; Wang et al., 2014). Using the transwell flow chamber, we found that 15-60 min IF treatment enhanced the phosphorylation of STAT6 at Tyr641, as well as STAT3 at both Tyr705 and Ser727 (Figure 2A). In contrast, IF treatment did not activate STAT1, a transcription factor for M1 polarization (Figure S4) (Wang et al., 2014). Collectively, these results illustrate that IF induces the M2 polarization of macrophages via the selective activation of M2-associated STAT3/6 pathway. Indeed, when we inhibited the phosphorylation of STAT3/6 with ruxolitinib (Figure S5), flow-induced mRNA and protein expression of M2 markers (Arg1 and TGF β) was drastically reduced (Figures 2B-D).

We next considered which molecules are responsible for flow-induced STAT3/6 activation and subsequent M2 polarization. We hypothesized that integrin could be involved in this process, since it governs the cells' interaction with their extracellular environment, and crosstalk between STAT and Src, which is a downstream effector of integrin, has been observed (Millward-Sadler et al., 2006; Silva, 2004). To test this hypothesis, we treated macrophages with Src inhibitor PP2, and subjected these macrophages to IF. We found that inhibiting Src significantly decreased flow-induced STAT3 and 6 phosphorylation (Figures 3A-B), as evident by the western blot quantification. Similar to the results of Src inhibition, blocking of β 1 integrin on these macrophages completely abrogated the flow-induced phosphorylation of STAT3 and 6 (Figures 3C-D), indicating that β 1 integrin and Src play important roles in IF-induced STAT3/6 activation. Collectively, these results (Figures 1-3) reveal that IF-induced macrophage M2 polarization is mediated via β 1 integrin/Src-dependent STAT3/6 activation.

IF enhances macrophages' ability to promote cancer cell migration

Knowing that IF polarizes macrophages toward an M2 phenotype that is often associated with macrophages in the tumor microenvironment, we next examined whether IF-treated macrophages can recapitulate certain functions of these tumor-associated macrophage (TAM). We decided to focus on macrophage's ability to promote cancer cell invasion, as it is one of the first steps in the metastatic cascade. We pre-treated macrophages seeded inside the 3D collagen I ECM with $\sim 3 \mu\text{m/s}$ IF for 48 hrs, and then co-cultured these macrophages with cancer cells for an additional 24 hrs (treatment group). We first compared the ability of flow-conditioned macrophages to alter cancer cell morphology to that of macrophages that were not treated with flow (control group) (Figure S6A). We found that co-culture of MDA-MB-435S (MDA435) melanoma cells with IF-pretreated macrophages resulted in the elongation of cancer cells (consistent with a migratory phenotype) compared to the control group (Figure 4A). Indeed, quantification of cancer cell morphology showed that MDA435 cells, MDA-MB-231 (MDA231) breast cancer cells, and Du145 prostate cancer cells co-cultured with macrophages that were pretreated with IF have higher aspect ratio (Figure 4B) and lower circularity (Figure S6B) than cells co-cultured with macrophages that did not receive IF pre-treatment. This indicates that IF promotes macrophages' ability to enhance cancer cell elongation and protrusion formation in multiple types of cancer cells.

We then tested whether macrophages conditioned with IF have enhanced abilities to promote cancer cell migration. We first seeded MDA231 cancer cells inside a collagen I ECM, and we treated these cancer cells with conditioned media collected from macrophages pre-treated with $\sim 3 \mu\text{m/s}$ IF (Figure S6A). We then tracked the movement of these cancer cells in the 3D ECM and quantified their migration trajectories (Figure 4C). Two metrics were used to quantify cell migration: total speed and directedness (Figure 4D). Total speed is defined as the total distance that a cell travelled divided by migration time and measures how fast the cell moves. In contrast, directedness is defined as the ratio between the displacement of the cell and the total distance travelled, which measures the persistence, or the efficiency, of cell migration. We found that, compared to conditioned media collected from

macrophages that were not treated with flow, conditioned media from macrophages primed with IF significantly enhanced cancer cell migration total speed (from 5.9 ± 0.2 $\mu\text{m/hr}$ to 9.8 ± 0.2 $\mu\text{m/hr}$, mean \pm SEM, $p < 0.001$) and directedness (from 0.13 ± 0.01 to 0.22 ± 0.02 , mean \pm SEM, $p < 0.001$), allowing cancer cells to migrate faster and more efficiently in the 3D ECM (Figure 4E). We then tested whether this enhancement in cancer cell migration is due to the flow-induced macrophage expression of TGF β , which can promote cancer cell migration (Xu et al., 2009). Conditioned media collected from macrophage pre-treated with flow were incubated with blocking antibodies against TGF β . We found that inhibiting TGF β in the conditioned media drastically reduced its ability to promote cancer cell migration speed and directedness compared to IgG control (Figures 4E and S7). Taken together, these results show that IF promotes the pro-invasion phenotype of macrophages by enhancing macrophage expression of TGF β .

IF enhances macrophage migration in 3D ECM

We next tested whether IF can enhance macrophage migration in 3D ECM, as the ability of macrophages to infiltrate into the tumor microenvironment critically depends on their ability to navigate through the extracellular matrix. Using the microfluidic device, we treated macrophages that were seeded in a collagen I gel with 3 $\mu\text{m/s}$ IF for 18 hrs. We tracked the movement of these macrophages with time-lapse microscopy to map the cell migration trajectories and quantify the migration total speed and directedness as defined in Figure 4D. Cell trajectory plots (Figure 5A) and migration quantification (Figure 5B) reveals that IF treatment significantly enhanced both migration total speed and directedness of bone marrow-derived macrophages (BMDM) and Raw 264.7 macrophages (Raw) over no-flow controls, allowing these macrophages to migrate faster and more persistently in the 3D ECM.

We also directly compared the migration characteristics of IF-treated macrophages with that of macrophages that were induced to an M2 phenotype with chemical stimuli. We first treated macrophages with LPS or IL4 to chemically induced them to an M1 or M2 phenotype, respectively. Using the microfluidic device, we then measured the total speed and directedness of these macrophages migrating

within the collagen I ECM. It should be noted that no interstitial flow treatment was imposed upon these macrophages that were treated with chemical factors (LPS or IL4). Similarly, no external chemical stimulus was applied to macrophages that were treated with interstitial flow. We found that, consistent with previous reports (Hind et al., 2016; Zhang et al., 2013a), IL4-treated M2 macrophages have higher migration total speed and directedness compared to control (no treatment, naïve, M0 macrophages) and LPS-treated M1 macrophages. More importantly, both migration total speed and directedness of the IL4-treated M2 macrophages were found to be similar to that of flow-treated macrophages (Figure S8), indicating the flow-enhanced macrophage migration may be a direct consequence of interstitial flow-induced M2 polarization.

Since Akt and FAK phosphorylation is frequently associated with enhanced motility and M2 polarization in macrophages (Chen et al., 2014; Miao et al., 2016; Vergadi et al., 2017; Yu et al., 2015), we conducted experiments in the transwell flow chamber to determine if IF could induce the activation (phosphorylation) of these two kinases in macrophages. We found that, compared to no-flow control, 1-hr IF treatment induced 2-3 fold increases in the phosphorylation of Akt and FAK at Ser473 and Tyr397, respectively (Figure 5C), providing further evidence that IF promotes M2 polarization. Moreover, inhibiting $\beta 1$ integrin led to a reduction in this flow-induced phosphorylation of Akt and FAK (Figure S9), similar to the responses observed for M2-associated transcription factors STAT3/6. Taken together, these results (Figures 5, S5 and S6) suggest that IF-enhanced migration of macrophages may be the result of $\beta 1$ integrin-mediated IF-induced M2 polarization.

IF directs macrophage migration against flow

Upon a closer examination of time-lapse images of macrophage migration, we noticed that IF biased macrophage migration against the flow direction (upstream) (Figure 6A). To verify this upstream migration behavior, we treated macrophages seeded in the microfluidic device with $\sim 3 \mu\text{m/s}$ and plotted the resulting migration vectors in a polar histogram plot (Rose plot). Rose plots reveal that more macrophages migrated against the direction of flow (Figure 6B). In fact, 85% of BMDM and 70% of Raw

macrophages migrated upstream under IF treatment compared to roughly an equal number (~50%) migrating in both directions for no-flow controls (Figure S10). To further quantify this upstream migration, we calculated forward migration index perpendicular (FMI_{\perp}) and parallel (FMI_{\parallel}) to the flow direction. FMI_{\perp} is calculated as the vector component of macrophage displacement perpendicular to the flow direction (D_{\perp}) divided by the total distance travelled (L). FMI_{\parallel} , on the other hand, is defined as the vector component of macrophage displacement against the flow direction (D_{\parallel}) divided by L , and it represents how persistently the macrophages migrate against the flow (Figure S11). Hence, a cell traveling upstream will have positive FMI_{\parallel} , while a cell traveling downstream will have a negative one. We observed that when treated with IF, macrophages migrated with positive FMI_{\parallel} for both BMDM and Raw cells. By comparison, macrophages that were not treated with flow have population average FMI_{\parallel} near zero, indicating no directional preference in migration. In addition, a quantification of FMI_{\perp} shows, as expected, no directional preference in migration perpendicular to the flow direction for both cell types ($FMI_{\perp} \sim 0$, Figure 6C). Finally, using the microfluidic device and high-resolution fluorescent confocal microscopy, we assessed the morphology of macrophages under IF treatment (Figure 6D). Quantification of the confocal images revealed that IF enhanced the formation of protrusions, as well as the accumulation of actin, on the upstream (flow-facing) side of the macrophages (Figures 6D and S12). Collectively, these results demonstrate that IF promotes the actin accumulation and protrusion formation favoring the flow-facing side of the macrophages, resulting in a preferential migration against the direction of flow (positive FMI_{\parallel}).

Discussion

Cells in the tumor microenvironment (TME) are constantly exposed to dynamic mechanical stimuli that influence cell behaviors and contribute to tumor progression (Heldin et al., 2004; Wirtz et al., 2011). Of particular importance is the role that interstitial flow (IF), a pathophysiologically relevant mechanical factor in tumors, plays in metastasis and tumor development. However, the effects of this tumor-associated flow on macrophages, the most abundant immune cells in the tumor tissues and a key

player in tumor progression (Condeelis and Pollard, 2006; Lewis and Pollard, 2006), have yet to be determined. Macrophages in the TME exist in various M2-like states. These macrophages are often considered tumor-supportive, suggesting that there may be therapeutic benefits in targeting these cells to reduce tumor progression and metastasis. Therefore, it is important to understand how IF affects these immune cells to gain a deeper insight into the tumor microenvironment. In this study, using biomimetic platforms that allow for the application of user-defined levels of IF through a 3D ECM, we demonstrated, for the first time, that macrophages can sense and respond to interstitial flow.

In contrast to previous studies that focus mainly on the effects of chemical factors on macrophage polarization, we show here that fluid flow can induce the polarization of macrophages toward an M2 phenotype as is evident from the up-regulation of various M2 markers (Arg1, CD206, and TGF β) in macrophages (Figure 1). These M2 markers are also over-expressed on tumor-associated macrophages (Afik et al., 2016; Krneta et al., 2017; Quatromoni and Eruslanov, 2012; Sharda et al., 2011; Zhang et al., 2017), indicating these flow-treated macrophages have a molecular signature that is similar to that of the macrophages in tumors. We further demonstrated that these flow-treated macrophages likely recapitulate certain functions of M2-like macrophages in tumors, in that they have enhanced capability to promote cancer cell migration, and they migrate faster than naïve (M0, untreated) or M1 macrophages (Figures 4 and 5). It is well known that macrophage polarization can be induced by chemical stimuli (growth factors and chemokines) or substrate topography (Mantovani et al., 2002; McWhorter et al., 2013). For instance, externally supplied cytokines such as IL4 and IL10 are known to induce the expression of M2 markers in macrophages. In contrast, LPS and IFN γ are used to initiate the production of macrophage M1 markers (Italiani and Boraschi, 2014). Our results are the first to demonstrate that interstitial fluid flow can polarize macrophages toward an M2 phenotype. Moreover, the finding that IF induces the production of TGF β by macrophages is significant in the context of tumor progression, since TGF β can promote epithelial-to-mesenchymal transition (EMT), cancer cell elongation, and cancer cell migration by down-regulating the expression of adhesion molecules (E-cadherin, ZO-1, and claudin) and up-regulating the

expression of MMPs in cancer cells (Lamouille et al., 2014; Xu et al., 2009). Indeed, our finding that interstitial flow enhances macrophages' ability to promote cancer cell elongation and migration (Figure 4) can be partially attributed to this flow-induced expression of TGF β in macrophages (Figure 1), as inhibiting TGF β in the conditioned media collected from IF-treated macrophages reduced cancer cell migration. Furthermore, TGF β promotes immune suppression by inhibiting the activation of cytotoxic T cells, NK cells, T helper cells, and dendritic cells while enhancing the generation of anti-inflammatory regulatory T (T_{reg}) cells (Arango Duque and Descoteaux, 2014; Noy and Pollard, 2014; Wrzesinski et al., 2007). In addition to TGF β , ArgI produced by macrophages can metabolize arginine, preventing it from inducing the expression of CD3 that is critical for T cell proliferation and proper function (Rodriguez et al., 2003). Finally, CD206 expressed on macrophages can dampen immune responses by scavenging molecules associated with inflammation (Lee et al., 2002). Therefore, our results suggest that interstitial flow-induced TGF β , ArgI, and CD206 expression by macrophages could contribute to tumor progression and invasion by promoting cancer cell migration and the suppression of immune responses.

We also report that flow-induced M2 polarization is mediated by the activation of the STAT3/6 pathway (Figure 2), leading us to conclude that this pathway is flow-sensitive in macrophages. It is known that externally supplied cytokines can activate STAT3/6 in macrophages (Jiang et al., 2000; Nakamura et al., 2015). Moreover, mechanical stretch has been reported to induce STAT3 phosphorylation in cardiomyocytes (Pan et al., 1999). However, this study is the first to report that forces produced by flow can mechanically activate STAT3/6 in macrophages. We further demonstrate that β 1 integrin and Src are indispensable in this flow-induced STAT3/6 activation (Figure 3). This result is supported by the fact that considerable crosstalk between STAT and Src pathways has been reported (Silva, 2004). For example, Src has been shown to directly interact with STAT3 in IL-3 stimulated cells, and the activation of Akt/mTOR pathway, which is regulated by Src (Chen et al., 2001), can enhance the phosphorylation of STAT3 at multiple sites (Reddy et al., 2000; Zhu et al., 2015). Furthermore, Src and Akt are known to be activated by FAK downstream of β 1 integrin (Larsen et al., 2003), as integrin

activation can contribute to the auto-phosphorylation of FAK at Tyr397, leading to downstream activity of Src/Akt (Guo and Giancotti, 2004; Mitra et al., 2005). This points to the possibility that FAK/Src/Akt relays the flow-induced signals to the M2-associated transcription factors STAT3/6. Indeed, we observed that, similar to STAT3/6, IF enhances the phosphorylation of Akt and FAK in macrophages via a β 1 integrin-dependent process (Fig. 5 and Fig. S9). Therefore, our results strongly suggest that mechanotransduction pathways containing β 1 integrin, Src/Akt/FAK, and STAT3/6 are responsible for the flow-induced M2 polarization of macrophages.

We reveal that IF enhances the migration of macrophages in 3D ECM. In fact, flow-treated macrophages have similar migration speed (total speed) and persistence (directedness) as that of macrophages chemically polarized to M2 phenotype via IL4 treatment, providing further evidence that flow-treated macrophages are phenotypically M2-like (Figure S8). Consistent with this observation, we found that IF increases the phosphorylation of FAK and Akt, kinases that are activated in M2 macrophages (Chen et al., 2014; Vergadi et al., 2017) and are known to promote macrophage motility (Miao et al., 2016; Yu et al., 2015; Zhang et al., 2013b). Furthermore, our results strongly suggest that IF could contribute to tumor progression by promoting macrophage migration, as enhanced motility of macrophages has been known to contribute to the development of tumors in several ways. Besides allowing macrophages to infiltrate into the tumor tissues and thus influence cancer cells that reside there, several studies have shown that macrophage movement can generate micro-tracks in the ECM, facilitating cancer cell invasion through these tracks (Guet et al., 2011). In addition, evidence gained from intravital imaging has shown that macrophages and breast cancer cells migrate in a co-dependent manner, and that inhibiting the migration of macrophages results in a reduction in the movement of cancer cells (Roussos et al., 2011). Lastly, macrophages have been shown to migrate into the perivascular space to assist in cancer cell intravasation by directly interacting with the vasculature (Dovas et al., 2013; Hughes et al., 2015; McKeever and Balentine, 1978).

Finally, we demonstrate that IF can direct the migration of macrophages in the upstream direction. Migration against the flow was previously reported for cancer cells and endothelial cells (Polacheck et al., 2014; Song and Munn, 2011; Vickerman and Kamm, 2012). In this study, we extend this observation, for the first time, to immune cells such as macrophages. Polacheck et al. have shown that IF promotes the migration of cancer cells against flow through flow-induced activation of $\beta 1$ integrin and FAK located on the upstream side of cells (Polacheck et al., 2011, 2014). Moreover, previous reports have shown that T cells that have adhered to the endothelium can crawl against the direction of the shear flow in the blood vessels, and this phenomenon is controlled by endothelial adhesion molecule ICAM-1 and 2 (Steiner et al., 2010). Since we found that flow-induced FAK and Akt phosphorylation in macrophages was controlled by $\beta 1$ integrin, we suspect that localized activation of integrin at the upstream side of macrophages could account for the preferential migration of macrophages against flow. More importantly, macrophage migration against the direction of IF could have implications for tumor progression. *In vivo*, numerous macrophages reside in the stromal tissues surrounding the tumor (Leek et al., 1996; Ohno et al., 2004; Wyckoff et al., 2007). Since interstitial fluid flows from the tumor tissue toward tumor-associated stroma (Heldin et al., 2004; Swartz and Lund, 2012), the observation that macrophages migrate against the flow suggests that IF, in addition to chemoattractants secreted by cancer cells (Condeelis and Pollard, 2006; Quail and Joyce, 2013), could act as a stimulus to guide macrophage infiltration into the tumor masses.

In summary, we propose a new framework whereby interstitial flow contributes to tumor progression by promoting macrophage M2 polarization and recruitment toward tumor tissues. Interstitial flow, through $\beta 1$ integrin/Src-mediated activation of STAT3/6, promotes macrophage transition to an M2 phenotype evident by flow-induced Arg I, TGF β , CD206, TGM2, and CD163 expression. This flow-induced M2 polarization enhances macrophage migration, as well as the ability of macrophages to promote cancer cell motility (Figure 7A). Moreover, IF also induces the preferential migration of macrophages against the direction of flow. Since interstitial fluid flows from the tumor mass to the

draining lymph nodes in tissues surrounding the tumor, macrophages in the surrounding stromal tissues could be directed by this flow to migrate upstream and infiltrate toward the tumor site. As interstitial flow induces macrophage M2 polarization, these macrophages could then produce chemical factors, such as TGF β and Arg I, to promote EMT, immunosuppression, and cancer cell invasion (Figure 7B). Taken together, our findings provide novel insights into the mechanobiology of macrophages and suggest that IF could play a key role in shaping the immune environment.

Material and Methods

Cell culture and reagents

Bone marrow-derived macrophages (BMDM) were generated from bone marrow cells isolated from fresh femur of 6-8 week old C57BL/6 mice. These bone marrow cells were subsequently cultured in RPMI (Invitrogen) supplemented with 10% fetal bovine serum (FBS, Invitrogen), 100 U/mL penicillin, 100 U/mL streptomycin, 1% HEPES (Invitrogen), 40 ng/mL MCSF (Peprotech) and 50 μ M β -Mercaptoethanol (Sigma) for 7 days to allow for the differentiation of macrophages according to a well-established protocol (Reedy et al., 2017; Zanoni et al., 2009). Raw 264.7 mouse macrophages (Raw), Du145 human prostate cancer cells (Du145), and MDA-MB-435S human melanoma cells (MDA435) were obtained from American Type Culture Collection (ATCC). MDA-MB-231 human breast carcinoma cells expressing GFP (MDA231) were kindly provided by Dr. Frank Gertler, MIT Department of Biology. Raw macrophages were cultured in DMEM (Invitrogen) supplemented with 10% heat-inactivated fetal bovine serum (HI-FBS, Invitrogen), 100 U/mL penicillin, and 100 U/mL streptomycin (Sigma). MDA435 cells and MDA231 cells were cultured in DMEM supplemented with 10% FBS, 100 U/mL penicillin, and 100 U/mL streptomycin. Du145 cells, on the other hand, were cultured in RPMI supplemented with 10% FBS, 100 U/mL penicillin, and 100 U/mL streptomycin. All cells were cultured in a humidified incubator operating at 5% CO₂ and 37 °C. Cell lines were authenticated using short tandem repeat profiling (Promega), and all cell lines tested negative for mycoplasma contamination. All antibodies used in this study were commercially available and validated by the vendors.

Microfluidic assay

Microfluidic System Design. To quantify the effects of interstitial flow (IF) on macrophage polarization and migration in 3D ECM, we used a poly-dimethylsiloxane (PDMS) microfluidic device consists of a bottom layer containing a microfluidic chamber and a top layer containing two large media reservoirs (Figures 1A and S1A). The microfluidic chamber is composed of a collagen gel region sandwiched between two micro-channels containing media. The gel region is separated from the micro-channels by an array of 10 PDMS micro-posts, five on each side. These micro-posts provide structure integrity to the collagen gel and, through surface tension, prevent the leakage of the gel into the channels during the polymerization process. Except for the micro-posts, the boundary of the collagen gel is in direct contact with the media in the micro-channels. The micro-channel and the collagen gel region both have the dimension of 2.31 mm in length, 500 μm in width, and 200 μm in height. The media channels in the bottom layer are connected to the media reservoirs in the top layer via media ports (Figure S1).

Device Fabrication. The PDMS microfluidic devices were assembled according to previously described methods using soft lithography (Polacheck et al., 2014). Briefly, PDMS pre-polymer (Dow Corning) was mixed with curing agent (Dow Corning) at a ratio of 10:1. The mixture was pour over a silicon wafer containing the features of the microfluidic chambers and cured overnight at 80 °C. The cured PDMS containing the features was removed from the silicon wafer, and the media and collagen gel filling ports were fabricated using a biopsy punch. The cured PDMS was then autoclaved and dried in the 80 °C oven. After overnight incubation, the microfluidic chamber was assembled by treating the sterile PDMS with plasma (Harrick Plasma) for 90 secs before binding it to a sterile coverslip (Corning).

Cell Seeding. 1.3×10^6 of BMDM or Raw 264.7 macrophages were suspended in a 2.5 mg/mL collagen I gel (Corning). The collagen gel-cell mixture was injected into the gel region of the microfluidic chamber (bottom layer) using a micropipette through the gel filling port. The gel-cell mixture was allowed to polymerize for 30 mins at 37 °C and pH of 8 in a humidified chamber. To prevent the cells from settling to the bottom of the device, the PDMS device was flipped during the polymerization process. This

ensures that cells distribute evenly throughout the gel region along the z-axis. Growth media were supplied to the micro-channels after the collagen gel polymerization, and the cells were incubated at 37 °C and 5% CO₂ overnight. For experiments designed to measure the migration characteristics of chemically induced M1 or M2 macrophages, the naïve macrophages were pre-treated with 20 ng/mL of LPS (Sigma) or 20 ng/mL of mouse IL4 (Peprotech), respectively.

Migration Assay. After overnight incubation, the PDMS chamber containing cells (bottom layer) was sealed against a PDMS layer containing two large (2.5 cm x 4 cm) media reservoirs (top layer) that were surface activated by plasma. A media height difference of 1.5 mm was established across the two reservoirs to establish a hydrostatic pressure difference of ~15 Pa. The media reservoirs are connected to the micro-channels via the media ports to allow the pressure gradient to transmit through the collagen gel containing the cells, resulting in the flow of media through the 3D collagen I ECM with a velocity of ~3 μm/s (interstitial flow). Darcy's law was used to calculate the media-height difference needed to induce an interstitial flow of ~3 μm/s through the 2.5 mg/mL collagen I ECM (*See Material and Methods, Hydraulic permeability estimation and interstitial flow calculation*).

The microfluidic device was then transferred to a light microscope (Zeiss) fitted with a humidified environmental chamber operating at 37 °C and 5% CO₂. The macrophages were treated with IF for a total of 18 hrs. Time-lapse microscopy was used to record the movement of macrophages in the 3D ECM. Phase contrast images were taken every 2 mins for 18 hrs with a focus at the mid-plane of the gel along the z-axis. Since the cross-sectional area of the reservoirs is 2000 times that of the gel region, the drop in the media-height difference during this 18-hr treatment was negligible. The media-height difference was measured after 18-hr treatment to verify that the height difference remained at ~1.5 mm.

Verification of flow velocity. To quantify the velocity of the IF, 200 nm FITC fluorescent micro-beads (Invitrogen) were introduced to the upstream reservoir (reservoir with higher pressure). The movement of the micro-beads through the collagen I ECM was recorded using a fluorescent microscope (Nikon). Image J (NIH) was used to track the bead movement, and Ibidi Chemotaxis and Migration software (Ibidi) was

used to quantify the velocity of beads flowing through the 3D ECM. Interstitial flow velocity after 18-hr flow treatment was measured to verify that the IF velocity remained at $\sim 3 \mu\text{m/s}$ throughout the course of the experiment.

Quantification of macrophage migration. Image J (NIH) was used to track the movements of the cells in the 3D ECM to produce cell trajectory plots. To ensure that macrophages had enough time to respond to IF, only the last 10 hrs of the 18 hrs movie were used for analysis. From the cell trajectory plots, we quantified macrophage migration total speed (total distance cell travelled divided by migration time), migration directedness (ratio between displacement and total distance travelled), forward migration index parallel (FMI_{||}) to the flow direction (vector component of macrophage displacement against the flow direction divided by total distance travelled), and forward migration index perpendicular (FMI_⊥) to the flow (the vector component of macrophage displacement perpendicular to the flow direction divided by the total distance travelled) using Ibidi Chemotaxis and Migration software (Ibidi) (Figures 4D and S11). Amounts of the cells that travelled upstream (against flow direction) and downstream (with flow direction) were also quantified. Finally, the angle of the displacement vector of each cell was quantified to generate polar histograms (Rose plots).

Immunofluorescent staining and confocal microscopy

4% para-formaldehyde (PFA, EMS) was perfused into the microfluidic devices to fix the cells in the collagen I ECM. To visualize the nucleus, the cells were stained with DAPI (diamidino-2-phenylindole, Sigma). The cells were also stained with Alexa-fluor 488 conjugated phalloidin (Invitrogen) to visualize actin. When appropriate, the fixed macrophages were stained with various antibodies to assess their polarization states. The fixed samples were first treated with Fc receptor blocking reagents (Miltenyi Biotec) to reduce nonspecific antibody binding. The cells were subsequently stained with anti-CD163 antibody (Abcam, Clone# EPR19518), anti-CD206 antibody (Abcam), and anti-CD86 antibody (Abcam), followed by appropriate secondary antibodies conjugated to fluorescent dyes

(Invitrogen). Confocal microscopy images of the cells were taken with Olympus confocal microscope fitted with a camera.

The confocal images were analyzed to quantify the distribution of the actin inside the macrophages as describe previously (Polacheck et al., 2014). Mid-plane of the cell was selected for image analysis. The image of the cell was divided at the centroid using an Image J script. The average fluorescent intensities of the actin at the upstream (flow-facing) $\langle I_{up} \rangle$ and downstream (away from flow direction) $\langle I_{down} \rangle$ sides of the cell were calculated. The actin distribution score (ADS) for each cell was quantified using the following formula:

$$ADS = \frac{\langle I_{up} \rangle - \langle I_{down} \rangle}{\frac{\langle I_{up} \rangle + \langle I_{down} \rangle}{2}}$$

Additionally, the same confocal images were analyzed to quantify the distribution of the protrusion as describe in previous studies (Polacheck et al., 2014). The image of the cell was divided at the centroid as before. The perimeters of the upstream side (P_{up}) and the downstream side (P_{down}) were quantified using Image J. The protrusion distribution score (PDS) of each cell was calculated as:

$$PDS = \frac{P_{up} - P_{down}}{\frac{P_{up} + P_{down}}{2}}$$

Finally, the fluorescent intensities of CD163, CD206, and CD86 in the stained macrophages were measured with ImageJ.

To test the effects of IF on the macrophage viability, macrophages were first treated with IF (~3 $\mu\text{m/s}$) for 48 hrs in the microfluidic device. Cell viability was subsequently assessed using live/dead viability kit (Invitrogen) according to the manufacturer's protocol.

Transwell flow assay

600,000 BMDMs or Raw macrophages were seeded in a 2.5 mg/mL collagen I gel contained inside a transwell insert (Falcon). The collagen scaffold containing the cells was allowed to polymerize in a humidified incubator for 30 mins at 37 °C and pH of 8. Following the polymerization, transwell inserts were placed into a six-well plate and supplied with growth media. The cells were cultured for 24 hrs in a humidified incubator at 5% CO₂ and 37 °C.

To treat macrophages with IF, growth media were added to the inside of the transwell insert to establish a media-height difference of 10 mm between the inside and outside of the insert. This media-height difference contributes to a hydrostatic pressure difference that drives a flow of 3 μm/s through the collagen gel containing macrophages in this transwell flow chamber. To maintain the hydrostatic pressure difference, a pump was connected to the transwell system that continuously re-circulated media from the outside of the insert back into the inside of the insert (Figure 1E). For the no-flow control group, same amount of media as the flow treatment group was added into the transwell system. However, instead of introducing media only into the inside of the insert, the media was distributed equally between outside and the inside of the transwell insert so that no media-height difference was established. This procedure is done to ensure that although flow treatment and no-flow control groups receive same amount of growth media, media-height difference will only be established in the treatment group. For the experiments that evaluated the effects of IF on protein expression, cells were treated with flow for 48 hrs. On the other hand, for experiments that evaluated the effects of IF on phosphorylation, cells were treated with flow for 15-60 min. When appropriate, macrophages in the transwell chambers were treated with 5 μM ruxolitinib (Invivogen), 20 μM PP2 (Abcam), 15 μg/mL anti-mouse β1 integrin antibody (Clone#HMb1-1, ebioscience), 15 μg/mL IgG isotype control antibody (Clone#299Arm, ebioscience), 20 ng/mL mouse IL4 (Peprotech), 20 ng/mL of mouse IFN γ (Peprotech) or dimethyl sulfoxide (DMSO, Sigma).

Hydraulic permeability estimation and interstitial flow calculation

The hydraulic permeability of the collagen gel scaffold determines the hydrostatic pressure gradient needed to achieve a desirable flow velocity. We used Darcy's law to estimate the hydraulic

permeability of 2.5 mg/mL collagen I gel scaffold in the microfluidic flow chamber according to protocols described in a previous study (Sudo et al., 2009). Briefly, plastic media reservoirs with small cross-sectional area were connected to the microfluidic device, and a media-height difference (Δh) of 1.5 cm was established to introduce a pressure drop across the 2.5 mg/mL collagen I gel scaffold. As the media flowed through the collagen gel, the drop in the media level in the high-pressure reservoir was monitored over time.

The relationship between pressure drop (ΔP) and volumetric flow rate (Q) across a collagen gel scaffold is described by Darcy's law:

$$\frac{Q}{A} = \frac{\Delta P(t) K}{W \mu} \quad (Eq. 1)$$

, where hydraulic permeability is K , viscosity is μ , surface area of the gel is A , and length of the gel scaffold in the direction of the flow is W (Sudo et al., 2009). Darcy's law can be transformed to model the change in volume of media in the reservoir (ΔV) over time. Using the plot of ΔV vs. time, we calculated hydraulic permeability (K) from the slope obtained from the linear regression analysis of the plot. Based on the measured change in media-height level and the geometry of the microfluidic device, the hydraulic permeability of the 2.5 mg/mL of collagen I gel scaffold was estimated to be $\sim 7 \times 10^{-14} \text{ m}^2$.

Darcy's law can also be transformed to describe the media-height difference (Δh_0) required to establish the pressure gradient to drive a desirable interstitial flow velocity (v) in the microfluidic device:

$$\Delta h_0 = \frac{v \mu W}{K \rho g} \quad (Eq. 2)$$

, where ρ is density of the media, and Δh_0 is the initial media-height difference of the reservoirs (Sudo et al., 2009). According to the geometry of the gel scaffold in the microfluidic device, as well as the hydraulic permeability of the scaffold estimated previously, the media-height difference needed to induce a $\sim 3 \text{ } \mu\text{m/s}$ interstitial flow in the microfluidic device was estimated to be 1.5 mm.

For transwell flow assay, a modified version of Eq. 2 was used to calculate the media-height difference (Δh_0) necessary to achieve a desirable interstitial flow velocity (v) in the transwell flow chamber:

$$\Delta h_0 = \frac{v\mu W}{K\rho g} + W \quad (\text{Eq. 3})$$

,where W is the thickness of the 2.5 mg/mL collagen I gel scaffold in the transwell. Based on this equation and the geometry of the transwell, the media height difference needed to establish a 3 $\mu\text{m/s}$ interstitial flow in the transwell flow chamber is ~ 10 mm.

Protein isolation and western blot analysis

Protein was extracted from the cells in the transwell flow chamber. Collagen I gel containing cells was washed two times with ice-cold 1X PBS and transferred into an Eppendorf tube. RIPA buffer (Cell Signaling) containing protease inhibitor (Sigma) and PMSF (Cell Signaling) was used to extract the cell lysates. A syringe was used to homogenize the gel to facilitate lysate extraction. We quantified the total protein concentration using BCA protein assay kit (Pierce) according to manufacturer's protocol. Equal amount of the total protein (30 μg -60 μg) was resolved on 4-12% NuPAGE electrophoresis gels (Invitrogen) and subsequently transferred onto nitrocellulose membranes (BioRad). The membranes were probed with rabbit anti-arginase I antibody (Thermo) at 1:1000, rabbit anti-TGF β antibody (Cell Signaling) at 1:1000, mouse anti-iNOS antibody (Cell Signaling) at 1:500, rabbit anti-CD206 antibody (Abcam) at 1:1000, rabbit anti-TGM2 antibody (Cell Signaling, Clone#D11A6) at 1:1000, rabbit anti-TNF α antibody (Cell Signaling) at 1:1000, rabbit anti-phospho STAT3 (Serine 727) antibody (Cell Signaling) at 1:1000, rabbit anti-phospho STAT3 (Tyrosine 705) antibody (Cell Signaling, Clone#D3A7) at 1:1000, rabbit anti-phospho Akt (Serine 473) antibody (Cell Signaling) at 1:1000, rabbit anti-phospho FAK (Tyrosine 397) antibody (Cell Signaling) at 1:1000, rabbit anti-phospho STAT6 (Tyrosine 641) antibody (Abcam) at 1:1000, rabbit anti-phospho STAT1 (Tyrosine 701) antibody (Cell Signaling, Clone#D4A7) at 1:500, mouse anti-STAT3 antibody (Cell Signaling, Clone#124H6) at 1:1000, rabbit

anti-STAT6 antibody (Cell Signaling, Clone#D3H4) at 1:1000, mouse anti-Akt antibody (Cell Signaling, Clone#40D4) at 1:1000, rabbit anti-FAK antibody (Cell Signaling) at 1:1000, rabbit anti-STAT1 antibody (Cell Signaling) at 1:1000, mouse anti- β actin antibody (Thermo, clone#BA3R) at 1:20,000, or mouse anti-GAPDH antibody (Thermo, clone#GA1R) at 1:20,000. After the primary antibody incubation, the membranes were incubated with appropriate secondary antibodies conjugated to horseradish peroxidase (Cell Signaling). ECL Chemiluminescent substrate (Invitrogen) was used to detect the immunoreactive band. Densitometry analysis, performed using Alpha Innotech (Alpha Innotech) software, was used to quantify western blot images. β -actin or GAPDH was used as loading control. When appropriate, stripping buffer (Thermo) was used to allow for the re-probing of nitrocellulose membranes.

Total RNA isolation and Real-time PCR

Total RNA was extracted from macrophages cultured in the collagen I gel using a tissue homogenizer (QIAshredder, QIAGEN) in combination with RNeasy Mini Kit (QIAGEN). mRNA expression was measured by real-time RT-PCR using SYBR Green Master Mixture and High-Capacity Reverse Transcription kit (Applied Biosystems). Comparative Ct method was used to analyze the data, with data normalized to β -actin expression in each sample. The sequences of primers used were: TGFB1-F: ATGCTAAAGAGGTCACCCGC; TGFB1-R: TGCTTCCCGAATGTCTGACG; ARG1-F: ATGGGCAACCTGTGTCCTTT, ARG1-R: TCTACGTCTCGCAAGCCAAT; ACTB-F: GGCTGTATTCCCCTCCATCG; and ACTB-R: CCAGTTGGTAACAATGCCATGT

Cancer cell morphology and migration experiment

600,000 macrophages were first seeded in a 2.5 mg/mL collagen I gel and then pretreated with IF for 48 hrs using transwell flow chamber. After the flow treatment, the transwell insert containing the macrophages was transferred into a well containing 200,000-300,000 MDA231, MDA435, or Du145 cancer cells so that the macrophages can be co-cultured with cancer cells. After 24-hr co-culture, cancer cells were fixed using 4% PFA and stained with DAPI and Alexa-fluor 488 conjugated phalloidin

(Invitrogen). Phase-contrast and fluorescent images of cancer cells were taken using a fluorescent microscope (Nikon) fitted with a camera. The aspect ratio and circularity of cancer cells were quantified using ImageJ (NIH) to assess the morphology of the cells.

600,000 macrophages were pretreated with IF for 48 hrs using the Transwell flow chamber. After the flow treatment, conditioned media were collected from the transwell. Meanwhile, 20,000 MDA231 GFP cells were seeded inside a 2.7 mg/mL collagen I ECM within a microfluidic device. These MDA231 cells were treated with the conditioned media from macrophages, and their migration was monitored using a fluorescent microscope (Zeiss) fitted with an environmental chamber operating at 5% CO₂ and 37 °C. Image J (NIH) was used to track cancer cell migration to produce cell trajectory plots. Ibidi Chemotaxis and Migration software (Ibidi) was used to calculate cell migration metrics such as total speed (total distance travelled divided by migration time) and directedness (ratio between the displacement of the cells and the distance that cell travelled). When appropriate, the conditioned media collected from macrophages pre-treated with interstitial flow were incubated with either 10 µg/mL of blocking antibody against TGF-β (Bio X Cell) or 10 µg/mL of IgG Control (Thermo).

Statistical analysis

We used GraphPad Prism 6.0 (GraphPad Software) to perform statistical analyses, with a P-value of <0.05 considered statistically significant. In all figures, ns represents not significant, * represents P < 0.05, ** represents P < 0.01, and *** represents P < 0.001. We used two-tailed student t-test. All data meet the assumptions and criteria for the student t-test. D'Agostino-Pearson omnibus normality test and F-test (GraphPad) were performed to ensure all data meet the normality and equal variance criteria. At least three independent experiment (biological replicates; n≥3) were performed for each experimental group. Sample sizes were chosen to meet current standard for *in vitro* biological experiments. No sample was excluded for analysis. Each microfluidic device or transwell flow chamber was randomly assigned to an experimental group for treatment. Investigators were blinded when assessing the data. A random number was assigned to a sample before assessing the outcome of the experiment, so the identity of the

experimental group in which the sample belongs to was not known to the investigator performing the analysis.

Acknowledgements

This work was supported in part by the US National Institutes of Health (NIH) grant U01 CA214381 (R. Li, R.D.Kamm). The authors thank Dr. William Polacheck, Dr. Douglas Lauffenburger, Dr. Emad Moeendarbary, and Dr. Michael Hemann for valuable advice.

Author Contributions

R.L., M.Z., and R.D.K. developed the concepts and designed the experiments. R.L., H.X., and H.A. developed methodology. R.L., J.C.S., H.X., and T.A.L performed experiment and acquired data. R.L., H.X., T.A.L, and H.A. analyzed results. R.L. and R.D.K wrote the manuscript. All authors edited the paper.

Conflict of Interest Statement

R.D.K. discloses a significant financial interest in AIM Biotech, a company that manufactures microfluidic systems of a design similar to those used in the present study.

Materials & Correspondence

Request for materials and correspondence should be addressed to Roger D. Kamm (rdkamm@mit.edu).

References

- Afik, R., Zigmond, E., Vugman, M., Klepfish, M., Shimshoni, E., Pasmanik-Chor, M., Shenoy, A., Bassat, E., Halpern, Z., Geiger, T., et al. (2016). Tumor macrophages are pivotal constructors of tumor collagenous matrix. *J. Exp. Med.* *213*, 2315–2331.
- Arango Duque, G., and Descoteaux, A. (2014). Macrophage cytokines: involvement in immunity and infectious diseases. *Front. Immunol.* *5*, 491.
- Chen, P.-C., Cheng, H.-C., Wang, J., Wang, S.-W., Tai, H.-C., Lin, C.-W., and Tang, C.-H. (2014). Prostate cancer-derived CCN3 induces M2 macrophage infiltration and contributes to angiogenesis in prostate cancer microenvironment. *Oncotarget* *5*, 1595–1608.
- Chen, R., Kim, O., Yang, J., Sato, K., Eisenmann, K.M., McCarthy, J., Chen, H., and Qiu, Y. (2001). Regulation of Akt/PKB activation by tyrosine phosphorylation. *J. Biol. Chem.* *276*, 31858–31862.
- Condeelis, J., and Pollard, J.W. (2006). Macrophages: obligate partners for tumor cell migration, invasion, and metastasis. *Cell* *124*, 263–266.
- Dovas, A., Patsialou, A., Harney, A.S., Condeelis, J., and Cox, D. (2013). Imaging interactions between macrophages and tumour cells that are involved in metastasis in vivo and in vitro. *J. Microsc.* *251*, 261–269.
- Guiet, R., Van Goethem, E., Cougoule, C., Balor, S., Valette, A., Al Saati, T., Lowell, C.A., Le Cabec, V., and Maridonneau-Parini, I. (2011). The process of macrophage migration promotes matrix metalloproteinase-independent invasion by tumor cells. *J. Immunol.* *187*, 3806–3814.
- Guo, W., and Giancotti, F.G. (2004). Integrin signalling during tumour progression. *Nat. Rev. Mol. Cell Biol.* *5*, 816–826.
- Haessler, U., Teo, J.C.M., Foretay, D., Renaud, P., and Swartz, M. a (2012). Migration dynamics of breast cancer cells in a tunable 3D interstitial flow chamber. *Integr. Biol. (Camb)*. *4*, 401–409.
- Heldin, C.-H., Rubin, K., Pietras, K., and Ostman, A. (2004). High interstitial fluid pressure - an obstacle in cancer therapy. *Nat. Rev. Cancer* *4*, 806–813.
- Hind, L.E., Lurier, E.B., Dembo, M., Spiller, K.L., and Hammer, D.A. (2016). Effect of M1–M2 Polarization on the Motility and Traction Stresses of Primary Human Macrophages. *Cell. Mol. Bioeng.* *9*, 455–465.
- Hompland, T., Ellingsen, C., Øvrebø, K.M., Rofstad, E.K., Lunt, S., Fyles, A., Hill, R., Milosevic, M., Heldin, C., Rubin, K., et al. (2012). Interstitial fluid pressure and associated lymph node metastasis revealed in tumors by dynamic contrast-enhanced MRI. *Cancer Res.* *72*, 4899–4908.
- Hughes, R., Qian, B.-Z., Rowan, C., Muthana, M., Keklikoglou, I., Olson, O.C., Tazzyman, S., Danson, S., Addison, C., Clemons, M., et al. (2015). Perivascular M2 Macrophages Stimulate Tumor Relapse after Chemotherapy. *Cancer Res.* *75*, 3479–3491.
- Italiani, P., and Boraschi, D. (2014). From Monocytes to M1/M2 Macrophages: Phenotypical vs. Functional Differentiation. *Front. Immunol.* *5*, 514.
- Jiang, H., Harris, M.B., and Rothman, P. (2000). IL-4/IL-13 signaling beyond JAK/STAT. *J. Allergy Clin. Immunol.* *105*, 1063–1070.
- Krneta, T., Gillgrass, A., Poznanski, S., Chew, M., Lee, A.J., Kolb, M., and Ashkar, A.A. (2017). M2-

polarized and tumor-associated macrophages alter NK cell phenotype and function in a contact-dependent manner. *J. Leukoc. Biol.* *101*, 285–295.

Lamouille, S., Xu, J., and Derynck, R. (2014). Molecular mechanisms of epithelial-mesenchymal transition. *Nat. Rev. Mol. Cell Biol.* *15*, 178–196.

Larsen, M., Tremblay, M.L., and Yamada, K.M. (2003). Phosphatases in cell–matrix adhesion and migration. *Nat. Rev. Mol. Cell Biol.* *4*, 700–711.

Lee, S.J., Evers, S., Roeder, D., Parlow, A.F., Risteli, J., Risteli, L., Lee, Y.C., Feizi, T., Langen, H., and Nussenzweig, M.C. (2002). Mannose Receptor-Mediated Regulation of Serum Glycoprotein Homeostasis. *Science* (80-). *295*, 1898–1901.

Leek, R.D., Lewis, C.E., Whitehouse, R., Greenall, M., Clarke, J., and Harris, A.L. (1996). Association of Macrophage Infiltration with Angiogenesis and Prognosis in Invasive Breast Carcinoma. *Cancer Res.* *56*, 4625–4629.

Lewis, C.E., and Pollard, J.W. (2006). Distinct role of macrophages in different tumor microenvironments. *Cancer Res.* *66*, 605–612.

Mantovani, A., Sozzani, S., Locati, M., Allavena, P., and A, S. (2002). Macrophage polarization: tumor-associated macrophages as a paradigm for polarized M2 mononuclear phagocytes. *Trends Immunol.* *23*, 549–555.

McKeever, P.E., and Balentine, J.D. (1978). Macrophages migration through the brain parenchyma to the perivascular space following particle ingestion. *Am. J. Pathol.* *93*, 153–164.

McWhorter, F.Y., Wang, T., Nguyen, P., Chung, T., and Liu, W.F. (2013). Modulation of macrophage phenotype by cell shape. *Proc. Natl. Acad. Sci.* *110*, 17253–17258.

Miao, L., Xin, X., Xin, H., Shen, X., and Zhu, Y.-Z. (2016). Hydrogen Sulfide Recruits Macrophage Migration by Integrin β 1-Src-FAK/Pyk2-Rac Pathway in Myocardial Infarction. *Sci. Rep.* *6*, 22363.

Millward-Sadler, S.J., Khan, N.S., Bracher, M.G., Wright, M.O., and Salter, D.M. (2006). Roles for the interleukin-4 receptor and associated JAK/STAT proteins in human articular chondrocyte mechanotransduction. *Osteoarthritis Cartilage* *14*, 991–1001.

Mitra, S.K., Hanson, D.A., and Schlaepfer, D.D. (2005). Focal adhesion kinase: in command and control of cell motility. *Nat. Rev. Mol. Cell Biol.* *6*, 56–68.

Nakamura, R., Sene, A., Santeford, A., Gdoura, A., Kubota, S., Zapata, N., and Apte, R.S. (2015). IL10-driven STAT3 signalling in senescent macrophages promotes pathological eye angiogenesis. *Nat. Commun.* *6*, 7847.

Nathanson, S.D., and Nelson, L. (1994). Interstitial fluid pressure in breast cancer, benign breast conditions, and breast parenchyma. *Ann. Surg. Oncol.* *1*, 333–338.

Niemand, C., Nimmegern, A., Haan, S., Fischer, P., Schaper, F., Rossaint, R., Heinrich, P.C., and Muller-Newen, G. (2003). Activation of STAT3 by IL-6 and IL-10 in Primary Human Macrophages Is Differentially Modulated by Suppressor of Cytokine Signaling 3. *J. Immunol.* *170*, 3263–3272.

Noy, R., and Pollard, J.W. (2014). Tumor-associated macrophages: from mechanisms to therapy. *Immunity* *41*, 49–61.

O’Sullivan, T., Saddawi-Konefka, R., Vermi, W., Koebel, C.M., Arthur, C., White, J.M., Uppaluri, R., Andrews, D.M., Ngiow, S.F., Teng, M.W.L., et al. (2012). Cancer immunoediting by the innate immune system in the absence of adaptive immunity. *J. Exp. Med.* *209*, 1869–1882.

- Ohno, S., Ohno, Y., Suzuki, N., Kamei, T., Koike, K., Inagawa, H., Kohchi, C., Soma, G.-I., and Inoue, M. (2004). Correlation of histological localization of tumor-associated macrophages with clinicopathological features in endometrial cancer. *Anticancer Res.* *24*, 3335–3342.
- Pan, J., Fukuda, K., Saito, M., Matsuzaki, J., Kodama, H., Sano, M., Takahashi, T., Kato, T., and Ogawa, S. (1999). Mechanical stretch activates the JAK/STAT pathway in rat cardiomyocytes. *Circ. Res.* *84*, 1127–1136.
- Panni, R.Z., Linehan, D.C., and DeNardo, D.G. (2013). Targeting tumor-infiltrating macrophages to combat cancer. *Immunotherapy* *5*, 1075–1087.
- Polacheck, W.J., Charest, J.L., and Kamm, R.D. (2011). Interstitial flow influences direction of tumor cell migration through competing mechanisms. *Proc. Natl. Acad. Sci.* *108*, 11115–11120.
- Polacheck, W.J., German, A.E., Mammoto, A., Ingber, D.E., and Kamm, R.D. (2014). Mechanotransduction of fluid stresses governs 3D cell migration. *Proc. Natl. Acad. Sci. U. S. A.* *111*, 2447–2452.
- Quail, D.F., and Joyce, J.A. (2013). Microenvironmental regulation of tumor progression and metastasis. *Nat. Med.* *19*, 1423–1437.
- Quatromoni, J.G., and Eruslanov, E. (2012). Tumor-associated macrophages: function, phenotype, and link to prognosis in human lung cancer. *Am. J. Transl. Res.* *4*, 376–389.
- Reddy, E.P., Korapati, A., Chaturvedi, P., and Rane, S. (2000). IL-3 signaling and the role of Src kinases, JAKs and STATs: a covert liaison unveiled. *Oncogene* *19*, 2532–2547.
- Reedy, J.L., Negoro, P.E., Feliu, M., Lord, A.K., Khan, N.S., Lukason, D.P., Wiederhold, N.P., Tam, J.M., Mansour, M.K., Patterson, T.F., et al. (2017). The Carbohydrate Lectin Receptor Dectin-1 Mediates the Immune Response to *Exserohilum rostratum*. *Infect. Immun.* *85*.
- Rodriguez, P.C., Zea, A.H., DeSalvo, J., Culotta, K.S., Zabaleta, J., Quiceno, D.G., Ochoa, J.B., and Ochoa, A.C. (2003). L-arginine consumption by macrophages modulates the expression of CD3 zeta chain in T lymphocytes. *J. Immunol.* *171*, 1232–1239.
- Roussos, E.T., Balsamo, M., Alford, S.K., Wyckoff, J.B., Gligorijevic, B., Wang, Y., Pozzuto, M., Stobezki, R., Goswami, S., Segall, J.E., et al. (2011). Mena invasive (MenaINV) promotes multicellular streaming motility and transendothelial migration in a mouse model of breast cancer. *J. Cell Sci.* *124*, 2120–2131.
- Sharda, D.R., Yu, S., Ray, M., Squadrito, M.L., De Palma, M., Wynn, T.A., Morris, S.M., and Hankey, P.A. (2011). Regulation of Macrophage Arginase Expression and Tumor Growth by the Ron Receptor Tyrosine Kinase. *J. Immunol.* *187*, 2181–2192.
- Silva, C.M. (2004). Role of STATs as downstream signal transducers in Src family kinase-mediated tumorigenesis. *Oncogene* *23*, 8017–8023.
- Song, J.W., and Munn, L.L. (2011). Fluid forces control endothelial sprouting. *Proc. Natl. Acad. Sci. U. S. A.* *108*, 15342–15347.
- Steiner, O., Coisne, C., Cecchelli, R., Boscacci, R., Deutsch, U., Engelhardt, B., and Lyck, R. (2010). Differential roles for endothelial ICAM-1, ICAM-2, and VCAM-1 in shear-resistant T cell arrest, polarization, and directed crawling on blood-brain barrier endothelium. *J. Immunol.* *185*, 4846–4855.
- Sudo, R., Chung, S., Zervantonakis, I.K., Vickerman, V., Toshimitsu, Y., Griffith, L.G., and Kamm, R.D. (2009). Transport-mediated angiogenesis in 3D epithelial coculture. *FASEB J.* *23*, 2155–2164.

- Swartz, M.A., and Lund, A.W. (2012). Lymphatic and interstitial flow in the tumour microenvironment: linking mechanobiology with immunity. *Nat. Rev. Cancer* *12*, 210–219.
- Vergadi, E., Ieronymaki, E., Lyroni, K., Vaporidi, K., and Tsatsanis, C. (2017). Akt Signaling Pathway in Macrophage Activation and M1/M2 Polarization. *J. Immunol.* *198*, 1006–1014.
- Vickerman, V., and Kamm, R.D. (2012). Mechanism of a flow-gated angiogenesis switch: early signaling events at cell-matrix and cell-cell junctions. *Integr. Biol. (Camb)*. *4*, 863–874.
- Wang, N., Liang, H., and Zen, K. (2014). Molecular mechanisms that influence the macrophage m1-m2 polarization balance. *Front. Immunol.* *5*, 614.
- Wirtz, D., Konstantopoulos, K., and Searson, P.C. (2011). The physics of cancer: the role of physical interactions and mechanical forces in metastasis. *Nat. Rev. Cancer* *11*, 512–522.
- Wrzesinski, S.H., Wan, Y.Y., and Flavell, R.A. (2007). Transforming growth factor-beta and the immune response: implications for anticancer therapy. *Clin. Cancer Res.* *13*, 5262–5270.
- Wyckoff, J.B., Wang, Y., Lin, E.Y., Li, J., Goswami, S., Stanley, E.R., Segall, J.E., Pollard, J.W., and Condeelis, J. (2007). Direct visualization of macrophage-assisted tumor cell intravasation in mammary tumors. *Cancer Res.* *67*, 2649–2656.
- Xu, J., Lamouille, S., and Derynck, R. (2009). TGF- β -induced epithelial to mesenchymal transition. *Cell Res.* *19*, 156–172.
- Yu, H., Littlewood, T., and Bennett, M. (2015). Akt isoforms in vascular disease. *Vascul. Pharmacol.* *71*, 57–64.
- Zanoni, I., Ostuni, R., and Granucci, F. (2009). Generation of mouse bone marrow-derived macrophages (BM-MFs). *Protoc. Exch.*
- Zhang, S., Che, D., Yang, F., Chi, C., Meng, H., Shen, J., Qi, L., Liu, F., Lv, L., Li, Y., et al. (2017). Tumor-associated macrophages promote tumor metastasis via the TGF- β /SOX9 axis in non-small cell lung cancer. *Oncotarget* *8*, 99801–99815.
- Zhang, Y., Sime, W., Juhas, M., and Sjölander, A. (2013a). Crosstalk between colon cancer cells and macrophages via inflammatory mediators and CD47 promotes tumour cell migration. *Eur. J. Cancer* *49*, 3320–3334.
- Zhang, Y., Wang, X., Yang, H., Liu, H., Lu, Y., Han, L., and Liu, G. (2013b). Kinase AKT controls innate immune cell development and function. *Immunology* *140*, 143–152.
- Zhu, Y.P., Brown, J.R., Sag, D., Zhang, L., and Suttles, J. (2015). Adenosine 5'-monophosphate-activated protein kinase regulates IL-10-mediated anti-inflammatory signaling pathways in macrophages. *J. Immunol.* *194*, 584–594.

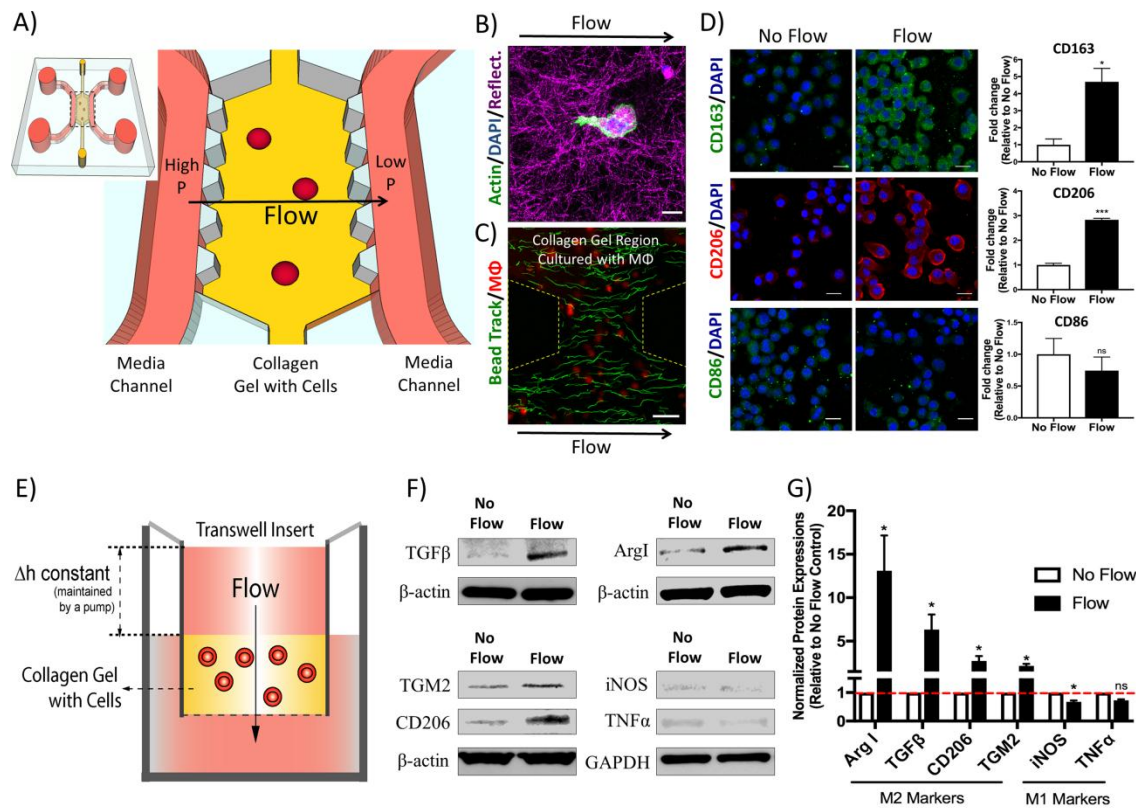


Figure 1: Interstitial flow (IF) promotes macrophage M2 polarization in 3D ECM. (A) Schematics of the microfluidic system used for IF study. Macrophages were suspended in the 3D collagen I ECM flanked by two microchannels containing media. A hydrostatic pressure gradient, which drives an IF of 3 $\mu\text{m/s}$ through the macrophage-containing ECM, was established between the two media channels by maintaining a media-height difference (see also Figure S1). (B) Representative fluorescent confocal image showing macrophage interacting with collagen I ECM (imaged by reflectance, magenta; scale bar=10 μm) in the microfluidic device. (C) Interstitial flow velocity in the microfluidic device was quantified by tracking the movement of 200 nm fluorescent microspheres (trajectories shown in green) as they flow through the collagen gel containing macrophages ($\text{M}\Phi$) labeled with Cell Tracker Red (red, scale bar=50 μm). (D) Immunofluorescence images (left, scale bars=20 μm) and quantification (right) showing that 48-hr of IF ($\sim 3 \mu\text{m/s}$) up-regulated the expression of M2 markers (CD 163 and 206) in bone-marrow derived macrophages (BMDM) cultured in the microfluidic device. The expression of M1 marker (CD86) was not significantly affected. (E) Transwell flow system used to study the effects of IF on macrophage protein expression. This system consists of a transwell chamber that is connected to a recirculating pump, maintaining a media-height and hydrostatic pressure differences that drive IF through collagen gel containing macrophages. (F-G) Western blot quantification (G) and representative images (F) showing that 48-hr of IF ($\sim 3 \mu\text{m/s}$) treatment up-regulated protein expression of M2 markers (Arg1, TGF β , TGM2, and CD206) in macrophages. The protein expression of M1 markers (iNOS and TNF α) was not significantly affected. Bars represent mean \pm standard error of mean (SEM) of data (fold change relative to no-flow control; n=3, n=number of independent experiments).

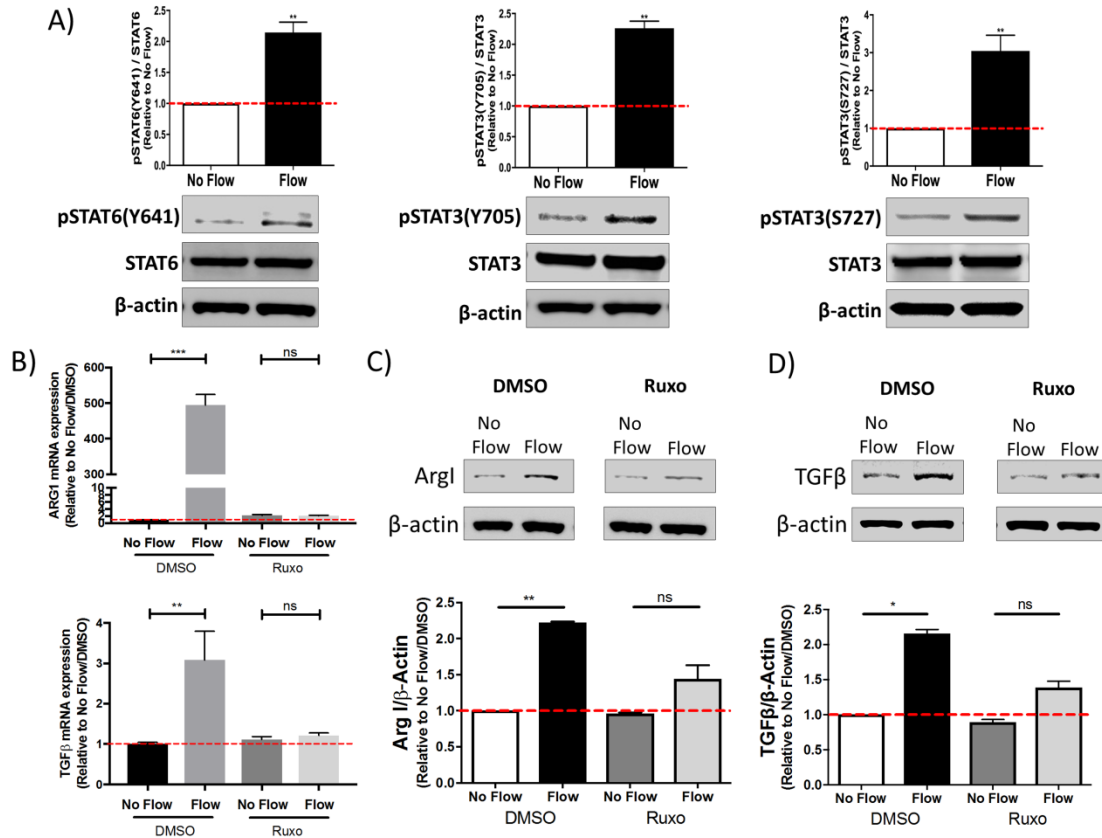


Figure 2: IF-induced macrophage M2 polarization is mediated by STAT3/6 activation. (A) Western blot quantification (top) and representative images (bottom) showing that 15 min of IF (3 μ m/s) treatment increased the phosphorylation of STAT6 at Tyr641 (left) and STAT3 at Tyr705 (center). In addition, 60-min IF treatment resulted in an increase in the phosphorylation of STAT3 at Ser727 (right). (B-D) Macrophages were treated with ruxolitinib (Ruxo, 5 μ M), an inhibitor of STAT3/6 phosphorylation, and subjected to IF treatment. Ruxolitinib diminished the flow-induced Arg I and TGF β mRNA (B) and protein expression (C-D) compared to DMSO controls. Bars represent mean \pm SEM of data (fold change relative to no-flow/DMSO control, n=3).

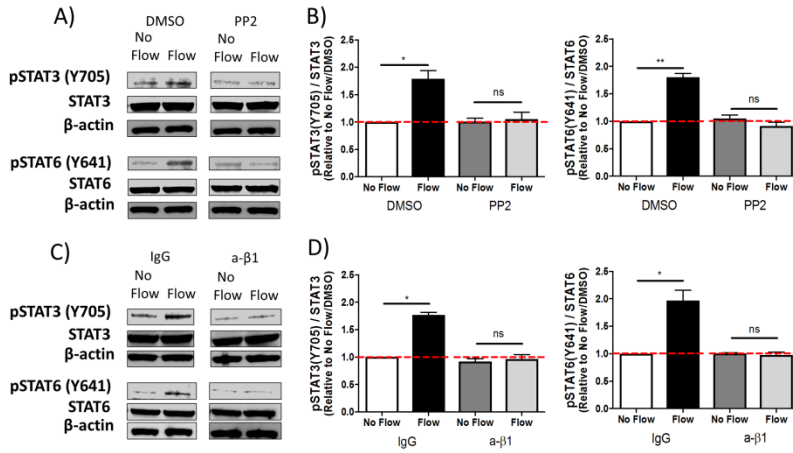


Figure 3: Src and $\beta 1$ integrin play crucial roles in flow-induced STAT3/6 activation. (A-B) Representative western blot images (A) and quantification (B) showing that the treatment of macrophages with Src inhibitor PP2 (20 μ M) abolished flow-induced STAT3 Tyr705 and STAT6 Tyr641 phosphorylation compared to DMSO control. (C-D) Representative western blot images (C) and quantification (D) showing that anti- $\beta 1$ integrin neutralizing antibody (15 μ g/mL) decreased flow-induced STAT3 Tyr705 and STAT6 Tyr641 phosphorylation compared to IgG isotype (15 μ g/mL) control. Bars represent mean \pm SEM of data (fold change relative to no-flow/DMSO control; n=3).

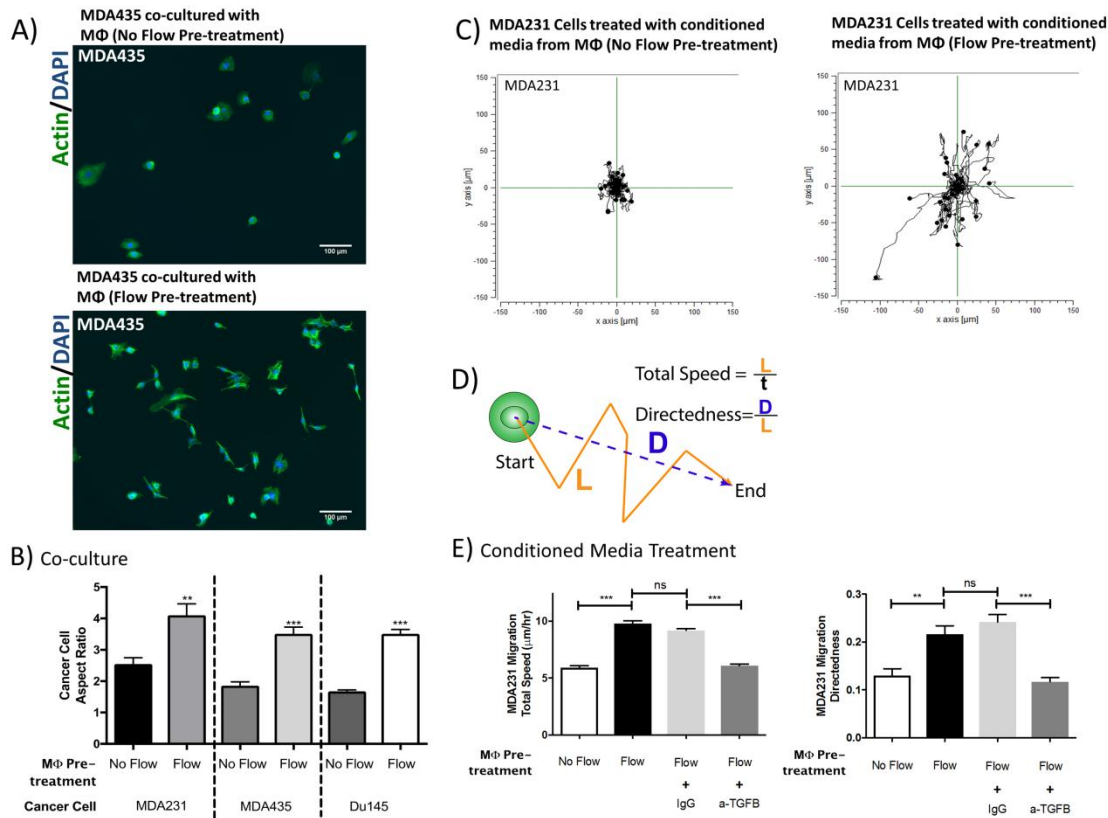


Figure 4: IF enhances the ability of macrophages to promote cancer cell migration. Murine bone marrow-derived macrophages were pre-treated with interstitial flow (3 $\mu\text{m/s}$ for 48 hrs) and their ability to influence cancer cell migration and morphology were assessed (see also Figure S6). **(A)** Representative fluorescent images (green=actin, blue=DAPI) showing that MDA435 cancer cells co-cultured with macrophages pre-treated with flow (bottom) were more protrusive than cancer cells co-cultured with macrophages that were not pre-treated with flow (top). **(B)** Quantification of cancer cell morphology showing that cancer cells co-cultured with macrophages pre-treated with flow have higher aspect ratio than ones co-cultured with control macrophages that were not treated with flow. **(C)** Representative migration trajectories of MDA231 cancer cells treated with conditioned media collected from macrophages pre-treated with flow (right) and of cancer cells treated with conditioned media from control macrophages (left). **(D)** Definition of cell migration dynamics. L =total migration distance; D =net displacement; t =time. Directedness is a measure of persistence. **(E)** MDA231 cancer cells treated with conditioned media from interstitial flow-primed macrophages show a higher migration total speed (left) and directedness (right) than cells treated with conditioned media from control macrophages. Inhibition of TGF β (anti-TGF β neutralizing antibody, 10 $\mu\text{g/mL}$) in the conditioned media reduced this increase in migration speed and directedness. Bars represent mean \pm SEM of data from 45-100 cells ($n=3$).

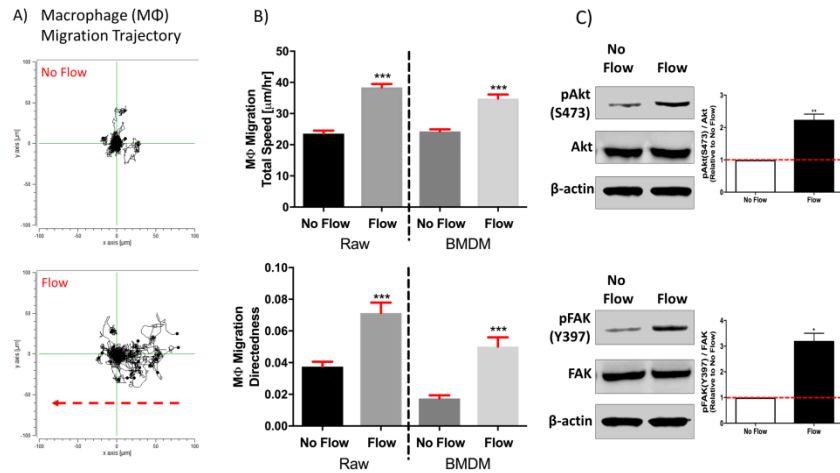


Figure 5: IF promotes macrophage migration in 3D ECM. (A) Representative migration trajectories of Raw macrophages in ECM under no-flow (top) and flow (bottom) conditions. The red arrow indicates flow direction. (B) 3 $\mu\text{m/s}$ IF increased macrophage migration total speed (top) and directedness (bottom) for both Raw macrophages and bone marrow-derived macrophages (BMDMs). Bars represent mean \pm SEM of data from 50-100 cells ($n=3$). (C) Western blot quantification (right) and representative images (left) showing that 1 hr of IF ($\sim 3 \mu\text{m/s}$) treatment up-regulated the phosphorylation of Akt at Ser473 (top) and FAK at Tyr397 (bottom) in macrophages. Bars represent mean \pm SEM of data (fold change relative to no-flow control; $n=3$).

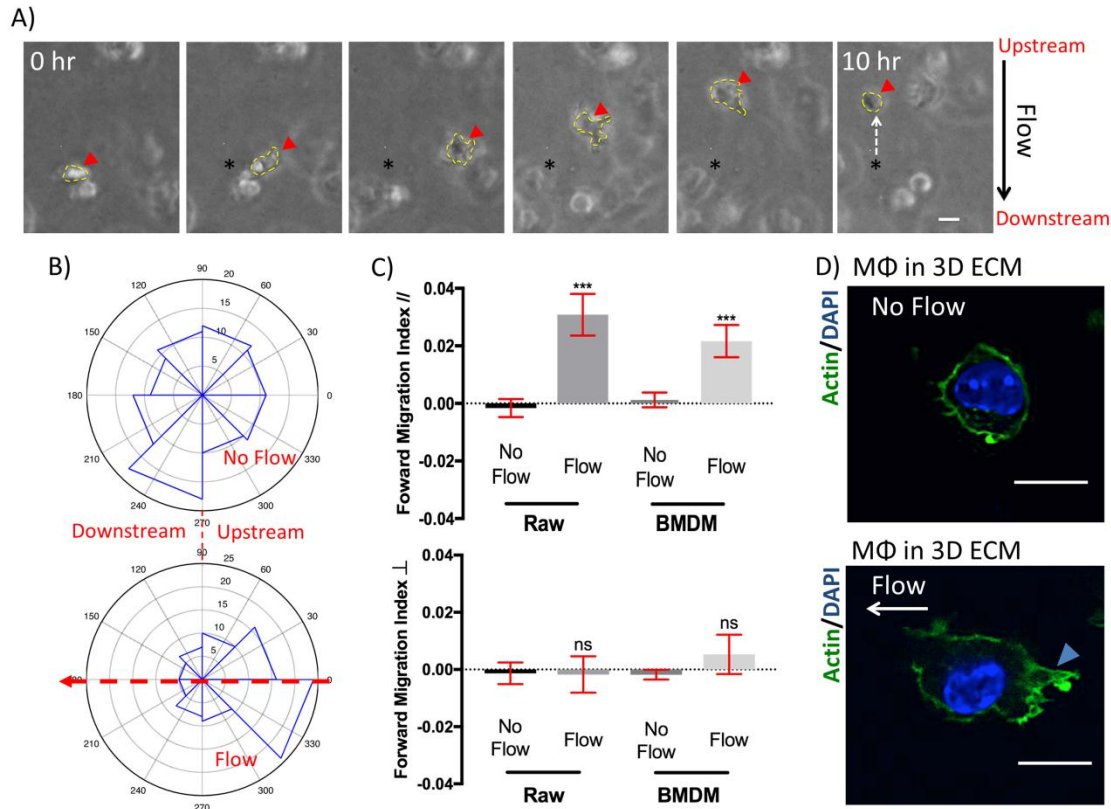


Figure 6: IF directs macrophage migration upstream. (A) Sample time-lapse image sequence showing macrophages migrating against the direction of interstitial flow (upstream) (red arrow=current location of the cell; black asterisk=initial location of the cell; yellow line=outline of the cell; white arrow points to the direction of cell migration, scale bar=30 μm). (B) Polar histogram showing the distribution of angles of net migration vectors for Raw macrophages in no-flow (top) and IF (bottom) conditions. The red arrow represents the direction of flow. Note that more macrophages migrated upstream (against the direction of the flow). (C) IF ($\sim 3 \mu\text{m/s}$) enhanced the forward migration index of Raw macrophages and BMDM in the flow direction (FMI_{//}, defined in Figure S11) but not perpendicular to the flow direction (FMI \perp). (D) Representative confocal fluorescent microscopy images (scale bar=10 μm) showing that actin localized to the periphery of the macrophages when cells were cultured in 3D ECM. IF ($\sim 3 \mu\text{m/s}$) treatment led to the accumulation of actin (green) and formation of protrusion (blue arrow) at the upstream (flow-facing) side of the macrophages (bottom). This is in contrast to no-flow control condition (top), in which no spatial preference in protrusion formation or actin accumulation was observed. Quantification is shown in Figure S12. Bars represent mean \pm SEM of data from 60-100 cells (n=3).

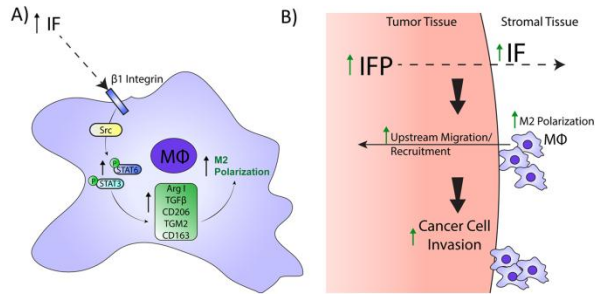


Fig. 7: Proposed models for the effects of interstitial flow (IF) on macrophages. (A) IF enhances macrophage M2 polarization via $\beta 1$ integrin/Src-mediated STAT3/6 activation. **(B)** IF can promote invasion by inducing macrophage M2 polarization and upstream migration. Tumor tissue has higher interstitial fluid pressure (IFP) than the surrounding stromal tissue, which drives an interstitial fluid flow from the tumor tissue to the stroma. This flow can induce the polarization of macrophages that reside in the stroma to a tumor-supportive, pro-invasion M2-like phenotype. Moreover, since IF induces upstream migration of macrophages, IF could promote these M2 macrophages to infiltrate into tumor tissue to drive tumor cell invasion, immune escape, and intravasation that could ultimately contribute to metastasis.